

The Close Binary Fraction of Dwarf M Stars

Benjamin M. Clark

Penn Manor High School, 100 East Cottage Avenue, Millersville, PA, 17551

California Institute of Technology, MSC 235, Pasadena, CA, 91126

Cullen H. Blake

*Princeton University, Department of Astrophysical Sciences, Peyton Hall, Ivy Lane,
Princeton, NJ 08544*

Gillian R. Knapp

*Princeton University, Department of Astrophysical Sciences, Peyton Hall, Ivy Lane,
Princeton, NJ 08544*

ABSTRACT

We describe a search for close spectroscopic dwarf M star binaries using data from the Sloan Digital Sky Survey (SDSS) to address the question of the rate of occurrence of multiplicity in M dwarfs. We use a template fitting technique to measure radial velocities from 145,888 individual spectra obtained for a magnitude-limited sample of 39,543 M dwarfs. Typically, the three or four spectra observed for each star are separated in time by less than four hours, but for $\sim 17\%$ of the stars, the individual observations span more than two days. In these cases we are sensitive to large amplitude radial velocity variations on time scales comparable to the separation between the observations. We use a control sample of objects having observations taken within a four hour period to make an empirical estimate of the underlying radial velocity error distribution and simulate our detection efficiency for a wide range of binary star systems. We find the frequency of binaries among the dwarf M stars with $a < 0.4$ AU to be 3 – 4%. Comparison with other samples of binary stars demonstrates that the close binary fraction, like the total binary fraction, is an increasing function of primary mass.

1. Introduction

The study of the orbital motions of stars in multiple systems has been an active area of research for more than a century (see Hearnshaw 1986). The fraction of stars which lie in

multiple systems (or conversely the fraction that are single), the dependence of these fractions on the mass of the primary, and the separation and mass ratio distributions of systems of multiple stars, are all observable quantities which can be measured through spectroscopic and imaging surveys and provide fundamental information in two important areas of stellar astrophysics. First, in certain circumstances observations of binary star systems directly measure the masses, radii, and luminosities of stars and provide the experimental bedrock for much of our theoretical understanding of the structure and evolution of stars. Second, surveys to determine the overall statistical properties of multiple systems within a population of stars help constrain their formation history; a detailed understanding of the fraction of binary stars across the HR diagram is an important part of a comprehensive picture of the process of star formation. To date, only a few measurements of the binary fraction and distribution for low-mass stars have been made - these stars are of low luminosity and the acquisition of the necessary large set of measurements is more difficult than for stars of higher mass and luminosity. They are of particular importance, however, because their formation and dynamical evolution within the systems in which they are born spans the mass range roughly between those of solar-type stars and planets.

The current understanding of star formation is that stars form in small-N clusters which are then broken apart by (short-term) dynamical decay and (longer-term) dynamical destruction (Goodwin et al. 2007). Due to the instability of multiple systems, some members of the system are likely to be ejected on a relatively short time scale; Anosova (1986) showed that in the vast majority of cases, the least massive star is ejected. On longer time scales, interactions with other stars in the star cluster disrupt binary stars (Goodwin et al. 2007). Both of these mechanisms predict that the multiplicity of stars should decrease to lower primary mass, but ejection is more important for close systems while interactions with other stars are more important for wide, loosely bound, systems.

The properties of multiple star systems with Sun-like primaries have received much attention of late. Recent work by Raghavan et al. (2010), which updates the seminal results of Duquennoy & Mayor (1991), found that Sun-like stars have an overall multiple fraction of $\sim 45\%$, with a log-normal distribution in separation that peaks around 60 AU. A similar analysis of lower mass M stars by Fischer & Marcy (1992) found a somewhat lower overall binary frequency of $42 \pm 9\%$. For objects straddling the stellar–brown dwarf boundary, Allen (2007) found that ultracool dwarfs (M6 and later) have a binary frequency of $20 \pm 4\%$, while Sana & Evans (2010) report that $\sim 75\%$ of O stars are binaries. Based on these results, Lada (2006) and Raghavan et al. (2010) point out that the overall fraction of single stars appears to be a decreasing function of stellar mass.

Fischer & Marcy (1992) report that $1.8 \pm 1.8\%$ of early-M stars are binaries with $0.04 \text{ AU} <$

$a < 0.4$ AU based on a sample of 62 stars, while Blake et al. (2010) report that $2.5^{+8.6\%}_{-1.6\%}$ of late-M and L dwarfs are binaries with $a < 1$ AU based on a sample of 43 objects. Extrapolating from the overall separation distribution functions presented by Raghavan et al. (2010) and Sana & Evans (2010) provides estimates that 3.7% and 26% of G and O stars are binaries with $a < 0.4$ AU, respectively. A complete view of stellar multiplicity across a wide range of separations, however, requires the use of a variety of observational techniques. Nearby systems with wide separations may be directly resolved using high resolution imaging, while systems with small separations are most readily detected as spectroscopic binaries. In particular, measuring the close binary fraction requires an extensive radial velocity (RV) survey of the type described by Raghavan et al. (2010).

Typically, individual multiple systems are identified in radial velocity surveys by fitting spectroscopic orbital solutions to velocity curves containing a large number of observations. Since close binaries are thought to be relatively rare for all but the most massive stars, a rigorous estimate of the multiplicity fraction requires a large number of observations of a large number of stars over long periods of time in order to detect an appreciable number of systems. This is particularly difficult for dwarf M stars because of their very low luminosities. An alternative approach is to use a small number of observations each for a very large number of stars to understand the rate of occurrence of multiple systems in a statistical sense (see Maxted & Jeffries 2005; Pourbaix et al. 2005). We take this approach in this paper, taking advantage of the enormous numbers of spectroscopic observations of M stars gathered during the course of the Sloan Digital Sky Survey (SDSS) to measure the close binary fraction of M stars using observations of 39,543 M dwarfs. While this data set is far larger than any used in previous research, it presents unique challenges. The data produced by the SDSS have significantly lower resolution and signal-to-noise ratio (S/N) than those typically used for making stellar velocity measurements. Additionally, SDSS typically only obtained three or four spectroscopic exposures of each object; in comparison, Fischer & Marcy (1992) obtained on average 15 observations per star. We demonstrate that an overall radial velocity precision of 4 km s^{-1} per observation can be achieved, more than sufficient for the detection of binary systems with short orbital periods, even with only few individual measurements. By quantifying the underlying statistical properties of the radial velocity measurements extracted from the SDSS spectra, and simulating the detection efficiency as a function of binary orbital separation and mass ratio, we make a robust measurement of the population of close binary M star systems.

2. SDSS Spectroscopic Data and Sample Selection

2.1. The Sloan Digital Sky Survey

The Sloan Digital Sky Survey (York et al. 2000) made an imaging and spectroscopic survey of the sky using a large-format CCD camera (Gunn et al. 1998) mounted on the Sloan Foundation 2.5 m telescope (Gunn et al. 2006) at the Apache Point Observatory, New Mexico, to image the sky in five optical bands - u , g , r , i , and z (Fukugita et al. 1996). The imaging data are reduced by a set of software pipelines which produce a catalog of objects with calibrated magnitudes and positions (Lupton et al. 2001, Lupton et al. 2003, Hogg et al. 2001). Targets for spectroscopy are selected from this catalog, mapped onto fiber plug plates (Blanton et al. 2003), and observed with two dual fiber-fed spectrographs (Uomoto et al. 1999) in a series of several 15-minute exposures. The spectra are optimally extracted, calibrated, combined (the *combined spectra*), and classified.

2.2. Selection of the M Star Sample

SDSS Data Release 7 (DR7: Abazajian et al. 2009) includes spectra of over 1.6 million objects, about 460,000 of which are stars. The parent M-star sample was selected from the spectroscopic data in DR7 by applying a series of cuts, first by magnitude and color ($z \leq 19.5$, $i - z > 0.2$ and $r - i > 0.5$). Next, data from plates with diffuse ionized gas emission and bad spectra (low S/N, missing data etc.) were removed, as were objects spectroscopically classified as stars earlier than K, as galaxies, or as quasars. The sample spectra were then examined by eye. Stars with obvious blue/white dwarf companions, stars superimposed on galaxies, and stars with the spectra of metal-poor (subdwarf M), K, or carbon stars were removed. The resulting sample (Knapp et al. in preparation) contains 51,193 individual M0-L0 stars with spectral types as defined by West et al. (2005).

2.3. Multiple SDSS Spectra

The SDSS usually obtained only one combined spectrum per object, but in a few cases there are two or more combined spectra, acquired one of two ways: (1) inadvertent observations of the same object on more than one spectroscopic plate, or (2) duplicate observations for quality check purposes, either of the same object on two plates or on the same plate, re-plugged and re-observed. These observations can be used to search for variability over periods from days to years, an example being the search by Pourbaix et al. (2005) for spectroscopic

binaries. In addition, the spectrum of each object is a combination of several exposures, and the spectra obtained from the individual exposures can also be used to search for variability, including radial velocity variability, as is done in the present paper.

The SDSS spectroscopic data are acquired as a series of spectroscopic exposures observed sequentially with an exposure time of 15 minutes each (*the individual 15 minute spectra*). These spectra are then averaged to produce the combined spectrum. The data are taken this way both to increase the dynamic range of the spectroscopic observations and to allow for the easy removal of data artifacts such as “cosmic rays”. Because of the scientific value of the individual spectra, software to reduce and calibrate them was prepared for release in DR7 along with the combined spectra. This data product is made available to enable studies of rapid spectral variability, since it provides, in almost all cases, three spectra observed with the same signal to noise ratio within a time period of one hour. The science enabled by these data includes identifying objects with short-period radial velocity variations such as compact degenerate binary pairs (Badenes et al. 2009), and the variability of the emission lines in dMe stars (Kruse et al. 2010; Hilton et al. 2010).

The typical exposure sequence is three fifteen-minute observations within a time span of about an hour. However, in marginal weather more exposures may be required to achieve the required S/N, or the observational sequence may be interrupted by variable weather conditions or instrumental problems. In other cases, the required S/N may not be achieved in a single night, and the individual observations are separated by significantly longer times. This enables searches for spectroscopic variability in the time domain, analogous to the photometric variability studies that have been carried out by Blake et al. (2008), Bhatti et al. (2010), and Becker et al. (2011). The present paper uses the individual spectra to search for radial velocity variations in the large sample of M stars defined above. We use only the observations from the same plugging of a plate (see (3) above) and do not consider the repeat observations of individual stars or plates (cases 1 and 2 above) - these are discussed elsewhere.

3. The Distribution of Radial Velocities

3.1. The Final Samples

We restricted the analysis to stars with $16 < i < 20.5$. We broke the sample into sub-samples based on Δt , the total time baseline spanned by the observations of an object: a *control sample* with $0 \text{ hr} \leq \Delta t \leq 4 \text{ hr}$ and an *experimental sample* with $2 \text{ d} \leq \Delta t \leq 30 \text{ d}$. We expect very few stars in the control sample to undergo significant accelerations on such

short time scales. We use the statistical properties of the radial velocity measurements of the objects in this sample as an empirical estimate of the underlying radial velocity error distribution. Among the set of objects with $2 \text{ d} \leq \Delta t \leq 30 \text{ d}$, the time spread between the observations is long enough that if the object is a close binary star we would observe significant radial velocity variations.

3.2. Calculation of Radial Velocities

We use a χ^2 minimization technique to estimate radial velocities from the SDSS spectra employing the average low-mass star templates from Bochanski et al. (2007) as a zero-velocity reference. Using a code written in Interactive Data Language (IDL), we determine the radial velocity that gives the best fit between the spectra and one of the templates by minimizing

$$\chi^2 = \sum_i \left[\frac{f_i - m(\lambda_i)}{\sigma_i} \right]^2 \quad (1)$$

where the sum is over all pixels in the spectrum (except for those flagged as bad, see below), f_i is the calibrated flux of the i^{th} pixel, $m(\lambda_i)$ is the value of the model at λ_i (the wavelength of the i^{th} pixel), and σ_i is the estimated standard deviation of f_i . We considered spectra only from the red arm of the SDSS spectrograph, which spans the region $\lambda = 5800 - 9200 \text{ \AA}$ at a resolution of $\lambda/\Delta\lambda \approx 1800$ and contains 2048 pixels (Stoughton et al. 2002). Since the templates provided by Bochanski et al. (2007) are normalized, there are two parameters that determine the model m that is the best fit for each spectrum: the radial velocity and an overall flux scaling. For each spectrum, we found the minimum of the χ^2 curve using an iterative process in which we tested velocities in the range $-1000 < RV < 1000 \text{ km s}^{-1}$ at a resolution of 1 km s^{-1} and then on a finer grid about the velocity found to have the smallest χ^2 in the previous step. This was repeated twice with the final step having a resolution of 0.1 m s^{-1} . The templates created by Bochanski et al. (2007) give values for the flux at 0.1 \AA intervals from 3825 \AA to 9200 \AA . For each test RV, the spectral template is interpolated onto a Doppler-shifted wavelength grid using cubic spline interpolation (Press et al. 1992). We fit each of the 11 templates (one for each spectral class from M0-L0) to each 15-minute spectrum of each star in our sample in order to find the best fitting template, and then select a single template that is used for all observations of a given target by finding the template that results in the lowest total χ^2 when fit to all of the observations of a given object. We correct for the barycentric motion of the Earth by applying velocity corrections produced by the SDSS pipeline.

During the fitting process, we exclude by down weighting spectral pixels that might

bias the resulting radial velocities. These include any pixels at wavelengths greater than $\lambda > 9150\text{\AA}$, any pixels in the $H\alpha$ emission region $6540 < \lambda < 6585\text{\AA}$, or pixels with the **BADSKYCHI** flag set by the SDSS pipeline. We exclude the reddest 50\AA of spectra since at these wavelengths telluric absorption and sky emission become significant and large radial velocity shifts may extend beyond the edges of the spectral templates. The $H\alpha$ emission line can be very strong in active M stars and is known to vary significantly even between individual observations of a given M star (Bochanski et al. 2007; Kruse et al. 2010), so we chose to exclude pixels within 22\AA of this feature. The **BADSKYCHI** flag indicates that sky emission lines are not being well fit by the SDSS spectral extraction pipeline, resulting in spectra that are potentially contaminated by sky emission.

3.3. Identifying Binaries

Given this sample of more than 145,000 radial velocity measurements, we hope to quantify our ability to detect short-timescale radial velocity variability in these data and estimate the rate of occurrence of short-period binary systems. Before doing this, we apply several cuts to the sample. We retain only radial velocity measurements from spectra that satisfy all of the following criteria: the average S/N of the pixels is greater than 10, the observation is not among the 10% of observations with the largest values of the χ^2 for the template fit, and after applying the two previous cuts, the spectra are of objects with at least three observations. We also remove objects from the sample that no longer fall into the definitions of our control and experimental samples due to the removal of observations by the previous cuts.

After applying these cuts, 23,031 observations of 7,059 objects remain in the control sample and 6,845 observations of 1,452 objects in the experimental sample; thus, of the final set of objects analyzed, 17% have observations with a time span of two days or more. In Figure 1 we show the distributions of the number of observations of each object and Δt for both samples, as well as the distributions of i -band magnitudes and $i - z$ colors.

For each of the objects in both samples, we define relative velocities, ΔRV_i ,

$$\Delta RV_i = RV_i - \frac{\sum_i RV_i \cdot (S/N)_i}{\sum_i (S/N)_i} \quad (2)$$

where RV_i and $(S/N)_i$ represent the RV, after applying the barycentric correction, and the average signal-to-noise ratio of all pixels of the i^{th} observation of the object, respectively. This is the difference between the radial velocity of the observation and the weighted average of the radial velocities of all observations where the weight function is $(S/N)_i$.

Given only a small number of observations of an object, it is extremely important to understand the underlying radial velocity error distribution if we hope to reliably detect radial velocity variations. For example, systematic sources of error can result in significant non-Gaussian tails to the error distribution that could produce spurious detections of radial velocity variability. Instead of relying on statistical estimates of the radial velocity error for a given measurement, we use the distribution of ΔRV derived from the control sample as an empirical error distribution.

We quantified the level of radial velocity variability for each object, x , as the sum of the absolute deviation of ΔRV

$$x = \frac{\sum_{i=1}^M |\Delta RV_i|}{M} \quad (3)$$

where M is the number of observations of the object. We ran a Monte Carlo simulation of 10^7 hypothetical sets of observations to determine a cutoff for x which is exceeded by only 10^{-3} of the simulated objects. For each simulated object, we chose the number of observations from the distribution of the number of observations of each object in the control sample. We then randomly chose the ΔRV values for each simulated object from the 23,031 actual ΔRV values in the control sample and calculated x using Equation 3. From the results of this simulation, we determined a cutoff value of $x > 10.4 \text{ km s}^{-1}$ for variability significant at the 10^{-3} level. Among the 1,452 objects in the experimental sample with $2 \text{ d} \leq \Delta t \leq 30 \text{ d}$, 22 exceed this cutoff and are therefore detected as radial velocity variables. These stars are listed in Table 1.

A histogram of the values of ΔRV computed for the control sample along with the best fit Gaussian distribution is shown in Figure 2. The standard deviation of the ΔRV values is 3.8 km s^{-1} , which compares favorably with the *rms* velocity error of 5.5 km s^{-1} at $g = 18.5$ and 12 km s^{-1} at $g = 19.5$ reported by Abazajian et al. (2009). However, there is a small set of objects with very large ΔRV values. Among the 7,059 objects in the control sample, 14 have at least one observation for which $\Delta RV > 20 \text{ km s}^{-1}$. This is far greater than would be expected if the values of ΔRV followed a Gaussian distribution. We examined the spectra of these objects individually, but all appear to be normal M dwarfs. However, we did note that many of the spectra contained a small number of highly errant pixels, likely due to cosmic rays, that were not fully down weighted by the SDSS pipeline. We considered the possibility that these errant pixels were dramatically altering the radial velocity fit and to test this hypothesis, we refit the spectra of the 22 detected binaries in the experimental sample and the 14 outliers in the control sample with the 5 most deviant pixels removed from the fit. We found that the radial velocity changed by an average of only 0.3 km s^{-1} , well within our radial velocity error, which allowed us to reject this explanation. Template mismatch also does not appear to be at fault as the average χ^2 of these objects

differs only slightly from the mean for the whole sample. Based upon this, we conclude that the objects are either in fact undergoing very short-term radial velocity variability, possibly due to a very tight binary system, or that there is an error in the wavelength calibration for these spectra. The wavelength solutions for each spectrum taken with each SDSS fiber are determined through a combination of fits to sky emission lines and arc lamp lines. As described by Abazajian et al. (2009), starting with DR7 these solutions were constrained to vary smoothly between fibers, resulting in overall calibration precision of $\pm 2 \text{ km s}^{-1}$ and significantly reducing the rate of errant solutions. Still, it is possible that rare problems with the wavelength solutions may be responsible for a small number of our measured RV shifts. In any case, these objects are of interest and warrant further observation. They are listed in Table 2. We also note that a significant percentage of Sun-like stars are known to be in higher-order multiple systems (34% doubles, 9% triples; Raghavan et al. 2010). We are only sensitive to short period systems, so even in a triple system we would only detect the reflex motion of the tight inner pair.

The raw numbers listed above show that 22 of the 1,452 stars (1.5%) in the experimental sample show statistically-significant radial velocity variations, compared to 14 of the 7,059 (0.20%) of the stars in the control sample. If the small number of large radial velocity variations in the control sample is due to some unidentified instrumental or analysis problem, we would also expect 0.20% of the experimental sample (3 stars) to show these variations; thus the raw binary fraction in the experimental sample is measured at the 7σ level (the on-average smaller number of observations available for the control sample is accounted for in the calculation of x in Equation 3).

3.4. The M Star Close Binary Fraction: a Bayesian Analysis

The raw binary star fraction of 1.5% derived above underestimates the true binary fraction which could in principle be measured by radial velocities of the accuracy available from the SDSS spectra, due to effects of inclination and the small number of observations of each star (see the discussion by Pourbaix et al. 2005). In this section, we use the radial velocity measurements of the stars in the control and experimental samples to estimate the true close binary fraction of the objects in our experimental sample by quantifying the number of objects that exhibit statistically significant radial velocity variations. To do this, we take a Bayesian approach to estimate the likelihood of a given close binary fraction given our observations and any prior information.

Let D represent the number of radial velocity variables detected, N_C a value for the close binary fraction, and B knowledge of any relevant background information about the

objects and the observations of the objects, such as their magnitudes and the times of the observations. Bayes' theorem states that

$$P(N_C|D, B) \propto P(D|N_C, B) \cdot P(N_C|B) \quad (4)$$

where $P(N_C|D, B)$, the probability of N_C given D and B , is the posterior distribution; $P(D|N_C, B)$, the probability of D given N_C and B , is the likelihood distribution; and $P(N_C|B)$, the probability of N_C given B , is the prior distribution for any N_C and D (Sivia & Skilling 2006).

As D represents the number of objects detected as radial velocity variables, it follows that

$$P(D|N_C, B) = \sum P(\{O_{i_1}, O_{i_2}, \dots, O_{i_D}\}|N_C, B) \quad (5)$$

where $P(\{O_{i_1}, O_{i_2}, \dots, O_{i_D}\}|N_C, B)$ is the probability that exactly the D objects, i_1, i_2, \dots, i_D , are detected as radial velocity variables and the sum is over all sets of D objects. Since whether or not one object is detected is independent of whether or not another object is detected,

$$P(\{O_{i_1}, O_{i_2}, \dots, O_{i_D}\}|N_C, B) = \prod_{j \in L} P(O_j|N_C, B) \cdot \prod_{j \notin L} P(\bar{O}_j|N_C, B) \quad (6)$$

where $L = \{i_1, i_2, \dots, i_D\}$, $P(O_j|N_C, B)$ is the probability that the j^{th} object is detected and $P(\bar{O}_j|N_C, B)$ is the probability that the j^{th} object is not detected. Substituting this into Equation 5 gives

$$P(D|N_C, B) = \sum \left[\prod_{j \in L} P(O_j|N_C, B) \cdot \prod_{j \notin L} P(\bar{O}_j|N_C, B) \right] \quad (7)$$

We must now consider how to calculate $P(O_j|N_C, B)$ and $P(\bar{O}_j|N_C, B)$. Following Maxted & Jeffries (2005) in assuming that the only cause of radial velocity variability is stellar multiplicity, it follows that the probability that the j^{th} object is detected as a radial velocity variable is $N_C p_{\text{detect},j} + (1 - N_C) \cdot 10^{-3}$ where $p_{\text{detect},j}$ gives the probability that we will detect the j^{th} object as a radial velocity variable if it is in fact a binary star. Note that the term $(1 - N_C) \cdot 10^{-3}$ arises from the fact that $1 - N_C$ is the probability that the object is not a binary star while 10^{-3} is the probability that an object will be detected as a radial velocity variable if it is not a binary star by the cutoff value of the variability metric we established to determine whether or not an object is a radial velocity variable. Thus, $P(O_j|N_C, B) = N_C p_{\text{detect},j} + (1 - N_C) \cdot 10^{-3}$ and $P(\bar{O}_j|N_C, B) = 1 - P(O_j|N_C, B) = 1 - [N_C p_{\text{detect},j} + (1 - N_C) \cdot 10^{-3}]$. We must now determine $p_{\text{detect},j}$ for each of the objects in the experimental sample, which can be done with a Monte Carlo simulation.

The radial velocity measurements described in section 3.3 and models for the distributions of system orbital parameters formed the basis of a Monte Carlo simulation designed to determine $p_{detect,j}$, which is required to generate the posterior distribution. This Monte Carlo simulation consisted of 10^5 virtual binary stars for each of the 1,452 objects in the experimental sample, which enabled us to estimate the efficiency with which we detect binaries given a wide range of different binary systems. For this simulation, we drew binary parameters from distributions based on previous results in the literature.

Semi-major axis, a : In order to have a reasonable chance to detect a binary in the experimental sample, there must be significant RV variations on the timescale of Δt , typically less than five days (Pourbaix et al. 2005). Since the stars we are looking at are M stars, $m_1 \sim m_2 < 0.5 M_\odot$, and we are able to detect large RV variations, say $\Delta RV > 20 \text{ km s}^{-1}$, we are primarily sensitive to very close systems with $a < 0.2 \text{ AU}$. Based upon our Monte Carlo simulations, we estimate that our average detection efficiency is 69% at $a = 0.1 \text{ AU}$ and 16% at $a = 0.4 \text{ AU}$. The distribution of the semi-major axes for systems with such small separations is not well known. We consider two different distributions of a . The first is a uniform distribution from 0.01 to 0.4 AU, while the second is a linear distribution such that $P(a) \propto a$ that also runs from 0.01 to 0.4 AU. Note that we might expect the uniform distribution to overestimate the value of $p_{detect,j}$ as the correct distribution should have a higher probability of larger separations and a corresponding lower probability of smaller separations (Allen 2007). This overestimate of $p_{detect,j}$ in turn implies that the best fit-binary fraction N_C will be underestimated.

Mass ratio, q : We follow Allen (2007) in using a power law distribution with a minimum of $q = 0.02$. Thus, if we let γ represent the power law index, the probability distribution function of q is

$$P(q) = \frac{q^\gamma}{\int_{0.02}^1 q^\gamma dq} \quad (8)$$

for $.02 < q < 1$ and $P(q) = 0$ for $0 < q < 0.02$. We test distributions with three different values for γ . We test $\gamma = 1.8$, as found by Allen (2007), and $\gamma = 1.2$ and 2.2, the extreme values on the 1σ confidence interval given by Allen (2007).

Primary mass, m_1 : Unfortunately, there is not a good method for determining the mass of the primary from the SDSS spectra as there are no well-calibrated mass-color or mass-luminosity relationships using the SDSS filters. Additionally, not knowing the metallicity or age of the star increases the uncertainty in determining its mass. However, this is not a major issue because, while the optical spectra and brightness of cool M dwarfs cover a large range, the corresponding mass range is modest, and we are able to obtain a rudimentary estimate of the primary mass using relations from the literature. Using the color transformations

provided by Davenport et al. (2006), from the apparent magnitude of the star in the r and i bands we can estimate the $i - J$ color. Also, using the color-magnitude relationships provided by West et al. (2005), we can determine the absolute magnitude, M_i from the $i - z$ color of the objects. Since $i - J = M_i - M_J$, we can estimate M_J . Finally, the mass-luminosity relations of Delfosse et al. (2000) allow for the estimation of the star’s mass from M_J . While the individual values of the mass obtained by these means have large systematic uncertainties, this is mitigated by selecting primary mass from a uniform distribution from 0.75 to 1.25 times the photometrically estimated mass in our Monte Carlo simulations.

Eccentricity, e : It is known that binaries with very short periods ($P < \sim 10\text{d}$) are highly likely to undergo tidal circularization (Duquennoy & Mayor 1991; Meibom & Mathieu 2005; Raghavan et al. 2010) and we can reasonably assume circular orbits, although the largest-separation pairs may have $e \neq 0$.

Orbital phase, f : The orbital phase at the time of the first observation is chosen from a uniform distribution from 0 to 2π .

Inclination, i : The inclination is chosen from a uniform distribution from 0 to π radians.

Longitude of periastron, ω : The longitude of periastron is chosen from a uniform distribution from 0 to 2π radians.

With our Monte Carlo simulation we generate hypothetical radial velocity curves for binary systems given the actual times of the observations of each object and Keplerian orbits given randomly selected system parameters from the above distributions. We estimate errors on the individual data points in the simulated radial velocity curves by randomly selecting values from the ΔRV distribution of our control sample. We can then compute x using Equation 3. If the value of x is greater than the cutoff value determined in section 3.3, 10.4 km s^{-1} , this system is tagged as detected. By running 10^5 trials for each of the 1,452 objects in our experimental sample and determining the fraction of trials in which we detect the simulated object, we estimate $p_{detect,j}$ as a function of the binary system parameters.

The prior distribution, $P(N_C|B)$, allows us to incorporate any relevant outside information into our analysis. We follow Allen (2007) in choosing a prior that assumes no outside knowledge and therefore is not biased towards any particular values of N_C . Thus, as N_C is a scale parameter, the proper prior to use is the Jeffreys’ prior (Sivia & Skilling 2006),

$$P(N_C|B) \propto \frac{1}{N_C}. \tag{9}$$

which is equivalent to uniform in the log of N_C .

Given the likelihood, $P(D|N_C, B)$, and prior distribution, $P(N_C|B)$, we can calculate the posterior distribution:

$$P(N_C|D, B) \propto P(D|N_C, B) \cdot P(N_C|B) \quad (10)$$

$$\propto \sum_{j \in L} \left[\prod_{j \in L} P(O_j|N_C, B) \cdot \prod_{j \notin L} P(\bar{O}_j|N_C, B) \right] \cdot \frac{1}{N_C} \quad (11)$$

$$\propto \sum_{j \in L} \left[\prod_{j \in L} [N_C p_{detect,j} + (1 - N_C)10^{-3}] \cdot \prod_{j \notin L} [1 - (N_C p_{detect,j} + (1 - N_C)10^{-3})] \right] \cdot \left(\frac{1}{N_C} \right)$$

We can then determine the constant of proportionality using the normalization condition

$$\int_0^1 P(N_C|D, B) dN_C = 1. \quad (13)$$

From this posterior distribution, we are able to determine the best fit value of the close binary fraction and a confidence interval on this value.

Table 3 gives the average value of $p_{detect,j}$ over all the objects and the best fit value of N_C and the 1σ confidence interval on N_C for each combination of a and q distributions. From Table 3, it is clear that changing the power law index γ has negligible impact on N_C . However, using a linear distribution for a as opposed to a uniform distribution increases N_C as expected, due to the decrease of $p_{detect,j}$ that results from using a distribution with a higher probability of large separations. The increase in N_C that results from using a linear distribution instead of a uniform distribution is 0.9%. Figure 3 shows the posterior distributions for the close binary fraction for both a uniform and linear distribution of a . Assuming the uniform distribution in a , the close binary fraction of the objects in our sample is $2.9_{-0.8}^{+0.6}\%$, while for a linear distribution in a we find $3.8_{-0.9}^{+0.9}\%$. We note that since our sample is magnitude limited, Branch bias (Branch 1976) may lead us to overestimate the rate of occurrence of multiple systems. For a population of binary systems with two identical stars, this can bias the measured binary fraction by up to 35%. We have not taken this into account in our analysis.

4. Results and Discussion

Previous work on the statistical properties of multiple star systems, such as that by Duquennoy & Mayor (1991) and Raghavan et al. (2010), has largely excluded M stars. Fischer & Marcy (1992) included spectroscopic binaries in their analysis of M star multiplicity and estimated that $\sim 1.8\%$ of M dwarfs are binaries with $0.04 \text{ AU} < a < 0.4 \text{ AU}$. This result, given that it is based on a very small sample of targets, is fully consistent with our estimate of the binary

fraction across a similar range of separations. The rate of occurrence of multiple systems, and the dependence of that rate on primary mass, may be an important observational clue to a unified theory of star formation. It has been shown by Lada (2006) and Raghavan et al. (2010) that the overall multiple fraction is a strong function of stellar mass, decreasing from near 80% at $10M_{\odot}$ to 20% for brown dwarfs with masses $< 0.1M_{\odot}$. We gathered values from the literature for the binary and close-binary fractions as a function of primary mass. These are listed in Table 4.

For the overall multiple fraction, N_T , we take the results of Allen (2007) for the brown dwarfs and lowest mass stars, Fischer & Marcy (1992) for M stars, Raghavan et al. (2010) for G stars, and Mason et al. (2009) and Sana & Evans (2010) for O stars, for which we assume an average primary mass of $40M_{\odot}$ based on the studies of O star eclipsing binaries by Weiden & Vink (2010). For the close binary fraction, N_C , of the lowest mass stars and brown dwarfs, we take the results from Blake et al. (2010) for the semi-major axis range $a < 1$ AU and scale down by a factor of 0.4 to estimate the binary fraction in the range $a < 0.4$ AU. For M stars we take the results presented here. For G stars we integrate the overall semi-major axis distribution from Raghavan et al. (2010), inferred from the period distribution by assuming binary systems with a total mass of $1.5M_{\odot}$, for $a < 0.4$ AU. For B stars we take the lower limit on the rate of occurrence of spectroscopic binaries with periods less than 10d derived by Mazeh et al. (2006) by applying the most extreme correction for the Branch bias to the result of Wolff (1978) and assume a stellar mass of $3.8M_{\odot}$. Finally, for O stars we use the empirical Cumulative Distribution Function (CDF) of observed O star spectroscopic binary periods to estimate N_C for $a < 0.4$ AU assuming the binaries have a total mass of $70M_{\odot}$, and therefore periods less than 10d. The relation between N_T and N_C and primary mass is shown in Figure 4.

These results show that the binary fraction is lower for lower mass stars across a wide range of orbital separations. However, the ratio N_C/N_T appears to increase with increasing primary mass, indicating that either the peak of the semi-major axis distribution moves to smaller values of a for larger stellar masses or that the overall shape of the separation distribution evolves significantly with primary mass. Based on well-studied samples of M/L and G stars, there is evidence that in fact the lowest mass binaries tend to have smaller separations (Duquennoy & Mayor 1991; Allen 2007; Raghavan et al. 2010). We caution that for O and B stars the multiplicity studies are not as observationally complete as those focusing on L and G stars, though with such high multiple fractions for these massive stars already reported in the literature it is unlikely that a significant population of wide separation systems remains undetected. Even if, as suggested by Kroupa (2011), there is a universal Initial Period Function (IPF) for all binary stars, the processes of dynamical destruction by stars external to bound stellar systems and dynamical decay, i.e. ejection by stars internal to

the stellar system, must play an important role in the evolution of binary properties (Heggie 1975, Hills 1975) and a wide range of binary properties for field stars may be expected.

5. Conclusions

Using a large set of spectroscopic observations of cool dwarf M stars from the SDSS that provide sparsely-sampled time series (typically 3-4 observations) we isolate 22 close spectroscopic binary candidates by radial velocity variability. Comparison with the radial velocity distributions of a control sample also from SDSS shows that we have detected the raw binary fraction at a 7σ level. The cadence of the observations, and the SDSS radial velocity accuracy, make us sensitive to close binaries, with separations less than about 0.4 AU. The detectability of spectroscopic binaries in the SDSS observations is evaluated using a large Monte Carlo simulation of the observational properties of the underlying population. Taking into account this detection efficiency and the total number of objects in our sample, the close binary fraction ($a < 0.4$ AU) of dwarf M stars is determined to be $2.9_{-0.8}^{+0.6}\%$ assuming a uniform prior on the distribution of orbital separation a . Our estimated close binary fraction of 3 – 4%, depending on the prior for a , is broadly consistent with earlier results on the statistical properties of low-mass multiple systems.

By comparing our measurement of the close binary fraction of M dwarfs to previous results in the literature, we have shown that the close binary fraction, like the overall binary fraction, is an increasing function of primary mass. This result has implications for the formation of, and the early dynamical evolution of, systems of low mass stars and indicates that the overall distribution of binary separations may be a strong function of stellar mass. In the future, the methods described in this work can be used to investigate the binary fraction in the whole sample of stars observed spectroscopically by SDSS – over 460,000 stars, mostly of types K, G and F, and members of the thick disk and halo.

6. Acknowledgments

The authors would like to thank an anonymous referee for thoughtful comments that helped to improve this manuscript. We also thank Jim Gunn, Craig Loomis, Steve Bickerton, Fergal Mullally and Robert Lupton for their extensive work on the SDSS spectroscopic pipeline and in particular for making available the calibrated individual 15-minute spectra. We also thank David Latham for helpful conversations that contributed to this work. CHB thanks the National Science Foundation for support via NSF postdoctoral fellowship AST-

0901918, and GRK thanks the NSF and NASA for support via grants NNX07AH68G and AST-0706938. We thank Princeton’s astrophysics department, in particular David Spergel, for strong support of the undergraduate research program, which supported this work.

Funding for SDSS and for SDSS-II was provided by the Alfred P. Sloan Foundation, the Participating Institutions, the National Science Foundation, the U.S. Department of Energy, the National Aeronautics and Space Administration, the Japanese Monbukagakusho, the Max Planck Society, and the Higher Education Funding Council for England. The SDSS is managed by the Astrophysical Research Consortium for the Participating Institutions.

REFERENCES

- Abazajian, K. N., et al. 2009, *ApJS*, 182, 543
- Allen, P. R. 2007, *ApJ*, 668, 492
- Anosova, J. P. 1986, *Ap&SS*, 124, 217
- Badenes, C., Mullally, F., Thompson, S. E., & Lupton, R. H. 2009, *ApJ*, 707, 971
- Becker, A. C. et al. 2011, *ApJ*, 731, 17
- Bhatti, W. A., Richmond, M. W., Ford, H. C., & Petro, L. D. 2010, *ApJS*, 186, 233
- Blake, C. H., Torres, G., Bloom, J. S., & Gaudi, S. 2008, *ApJ*, 684, 635
- Blake, C. H., Charbonneau, D., & White, R. J. 2010, *ApJ*, 723, 684
- Blanton, M. R., et al. 2003, *AJ*, 125, 2276
- Bochanski, J. J., West, A. A., Hawley, S. L., & Covey, K. R. 2007, *AJ*, 133, 531
- Branch, D. 1976, *ApJ*, 210, 392
- Davenport, J. R. A., West, A. A., Matthiesen, C. K., Schmieding, M., & Kobelski, A. 2006, *PASP*, 118, 1679
- Delfosse, X., Forveille, T., Ségransan, D., Beuzit, J.-L., Udry, S., Perrier, C., & Mayor, M. 2000, *A&A*, 364, 217
- Duquennoy, A., & Mayor, M. 1991, *A&A*, 248, 485
- Fischer, D. A., & Marcy, G. W. 1992, *ApJ*, 396, 178

- Fukugita, M., et al. 1996, *AJ*, 111, 1748
- Goodwin, S. P., Kroupa, P., Goodman, A., & Burkert, A. 2007, *Protostars and Planets V*, 133
- Gunn, J. E., et al. 1998, *AJ*, 116, 3040
- Gunn, J. E., et al. 2006, *AJ*, 131, 2332
- Hearnshaw, J. B. 1986, “The analysis of starlight: One hundred and fifty years of astronomical spectroscopy”, New York, Cambridge University Press
- Heggie, D. C. 1975, *MNRAS*, 173, 729
- Hilditch, R. W. 2001, “An Introduction to Close Binary Stars”, Cambridge, UK: Cambridge University Press
- Hills, J. G. 1975, *AJ*, 80, 809
- Hilton, E. J., West, A. A., Hawley, S. L., & Kowalski, A. F., 2010, *AJ*, 140, 1402
- Hogg, D. W., Finkbeiner, D. P., Schlegel, D. J., & Gunn, J. E. 2001, *AJ*, 122, 2129
- Kroupa, P. 2011, *A&A*, 529, 92
- Kruse, E. A., et al. 2010, *ApJ*, 722, 1352
- Lada, C, 2006, *ApJ*, 640, 63
- Lupton, R. H., et al. 2001, *ASP Conf. Ser.* 238, 269
- Lupton, R. H., et al. 2003, *Proc. SPIE*, 4836, 350
- Mason, B.D., Hartkopf, W.I., Gies, D.R., Henry, T.J., & Helsel, J.W. 2009, *AJ*, 137, 3358
- Maxted, P. F. L., & Jeffries, R. D. 2005, *MNRAS*, 362, L45
- Mazeh, T., Tamuz, O., & North, P. 2006, *MNRAS*, 367, 1531
- Meibom, S., & Mathieu, R. D. 2005, *ApJ*, 620, 970
- Pourbaix, D., et al. 2005, *A&A*, 444, 643
- Press, W. H., Teukolsky, S. A., Vetterling, W. T., & Flannery, B. P. 1992, “Numerical Recipes”, 2nd Edition, Cambridge: Cambridge University Press

- Raghavan, D., et al. 2010, ApJS, 190, 1
- Sana, H., & Evans, C. J. 2010, arXiv:1009.4197
- Sivia, D. S., & Skilling, J. 2006, “Data Analysis”, 2nd edition, Oxford University Press
- Stoughton, C., et al. 2002, AJ, 123, 485
- Uomoto, A., et al. 1999, BAAS, 31, 1501
- Weiden, C. & Vink, J.S. 2010, A&A, 524, 98
- West, A. A., Walkowicz, L. M., & Hawley, S. L. 2005, PASP, 117, 706
- Wolff, S. C. 1978, ApJ, 222, 556
- Vogel, H. C. 1901, ApJ, 13, 324
- York, D. G., et al. 2000, AJ, 120, 1579

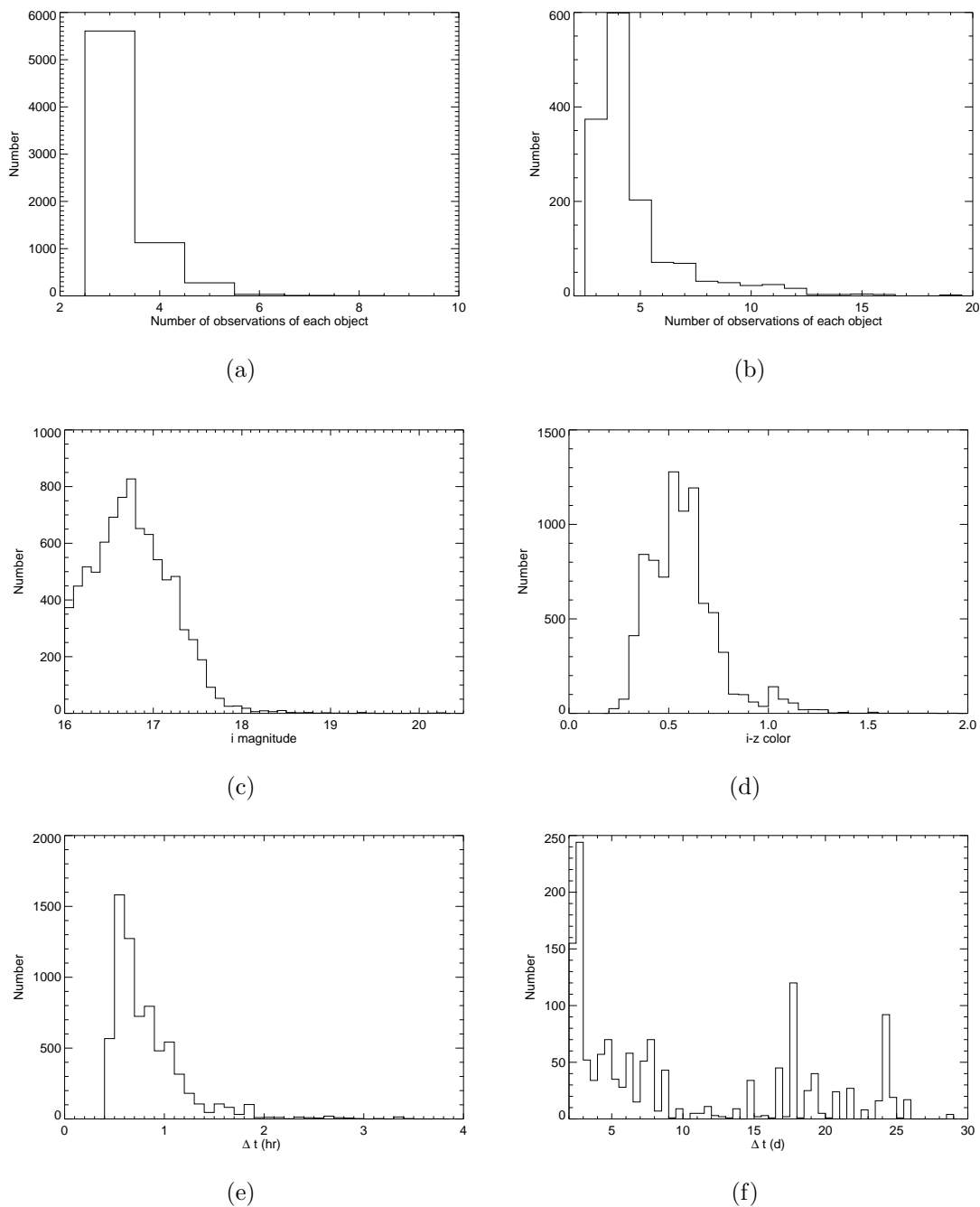


Fig. 1.—: Subfigures (a)–(f): histograms of the number of observations of each object in the sample with $0 \text{ hr} \leq \Delta t \leq 4 \text{ hr}$, the number of observations of each object in the sample with $2 \text{ d} \leq \Delta t \leq 30 \text{ d}$, the i magnitude in the combined sample, the $i-z$ color in the combined sample, Δt in the sample with $0 \text{ hr} \leq \Delta t \leq 4 \text{ hr}$, and Δt in the sample with $2 \text{ d} \leq \Delta t \leq 30 \text{ d}$, respectively.

Table 1. Object name, i magnitude, value of x calculated using Equation 3, the range in RV values ($RV_{range}=RV_{max} - RV_{min}$), and Δt for each object in the sample with $2 \text{ d} \leq \Delta t \leq 30 \text{ d}$ that we detected as a binary.

Object Name	i	x (km/s)	RV_{range} (km/s)	Δt (d)
SDSSJ002228.76–010806.9	16.59	12	38	19.002
SDSSJ004747.84–004550.5	17.02	17	38	17.938
SDSSJ010122.67–005311.6	17.07	14	35	2.019
SDSSJ011038.87–011409.5	17.31	12	32	6.013
SDSSJ011054.12+005227.4	16.54	14	37	6.013
SDSSJ074428.29+191554.7	17.47	70	251	5.035
SDSSJ074646.12+282629.9	17.55	12	44	7.056
SDSSJ083027.95+454736.5	17.33	13	35	4.184
SDSSJ083723.40+141211.1	16.95	11	26	14.936
SDSSJ084841.17+232051.7	16.34	92	202	8.090
SDSSJ105030.21+421451.4	16.44	24	90	3.004
SDSSJ105715.76+430945.9	16.33	24	97	3.015
SDSSJ114030.06+154231.5	16.18	47	98	17.963
SDSSJ114050.85+532304.0	16.65	13	35	24.966
SDSSJ115124.34+371953.8	16.37	14	40	2.135
SDSSJ121944.13+260759.8	16.13	12	36	2.865
SDSSJ163215.69+005918.6	16.66	24	98	24.994
SDSSJ163401.41+005010.0	16.87	14	53	24.994
SDSSJ204845.85+004001.3	17.47	47	182	19.957
SDSSJ212546.00–060858.6	16.12	16	43	22.955
SDSSJ220848.44+000409.9	17.12	23	59	20.869
SDSSJ225450.30–101003.2	17.17	17	40	21.975

Table 2. Object name, i magnitude, value of x calculated using Equation 3, the range in RV values ($RV_{range}=RV_{max} - RV_{min}$), and Δt for each object in the sample with $0 \text{ hr} \leq \Delta t \leq 4 \text{ hr}$ with at least one observation for which $\Delta RV > 20 \text{ km/s}$.

Object Name	i	x (km/s)	RV_{range} (km/s)	Δt (d)
SDSSJ003144.47+003033.6	17.49	14	40	0.758
SDSSJ021838.39+004946.8	16.98	16	41	0.685
SDSSJ072642.62+414243.2	16.64	14	44	1.188
SDSSJ075243.70+254928.3	17.39	15	41	0.723
SDSSJ082833.58+341531.6	16.79	15	35	0.554
SDSSJ085921.75+371147.9	18.19	15	34	1.087
SDSSJ092345.54+222432.4	16.56	48	133	1.242
SDSSJ111647.81+294602.7	16.24	14	36	0.585
SDSSJ125508.85+320849.9	17.04	10	33	1.053
SDSSJ143524.64+232249.5	16.97	17	48	0.564
SDSSJ154848.35+362803.7	17.04	17	42	0.438
SDSSJ163020.19+305254.5	16.62	20	55	1.343
SDSSJ163355.96+293725.0	16.98	13	34	1.343
SDSSJ163544.45+243032.3	16.78	13	35	1.873

Table 3. $\langle p_{detect,j} \rangle$, the best fit value of N_C and 1σ (68.3%) confidence interval on N_C for each combination of a and q distributions.

$P(a)$	$P(q)$	$\langle p_{detect,j} \rangle$	N_C
Uniform	$\gamma = 1.2$	0.45	$3.0^{+0.5\%}_{-1.0\%}$
Uniform	$\gamma = 1.8$	0.46	$2.9^{+0.6\%}_{-0.8\%}$
Uniform	$\gamma = 2.2$	0.47	$2.9^{+0.5\%}_{-0.9\%}$
Linear	$\gamma = 1.2$	0.34	$4.0^{+0.8\%}_{-1.1\%}$
Linear	$\gamma = 1.8$	0.35	$3.8^{+0.9\%}_{-0.9\%}$
Linear	$\gamma = 2.2$	0.36	$3.8^{+0.8\%}_{-1.0\%}$

Table 4. Summary of current results for the total binary fraction and close binary fraction for stars of various primary masses. See Section 4 for information on the sources of these values.

Primary Mass (M_\odot)	N_T (%)	N_C (%)
0.1	20	1.0
0.4	42	2.9
1.0	45	3.7
3.8	–	>8.0
40.0	75	26.0

Fig. 2.—: Histograms of ΔRV and $\Delta RV/\sigma$ for the control sample along with the best fit Gaussian distributions.

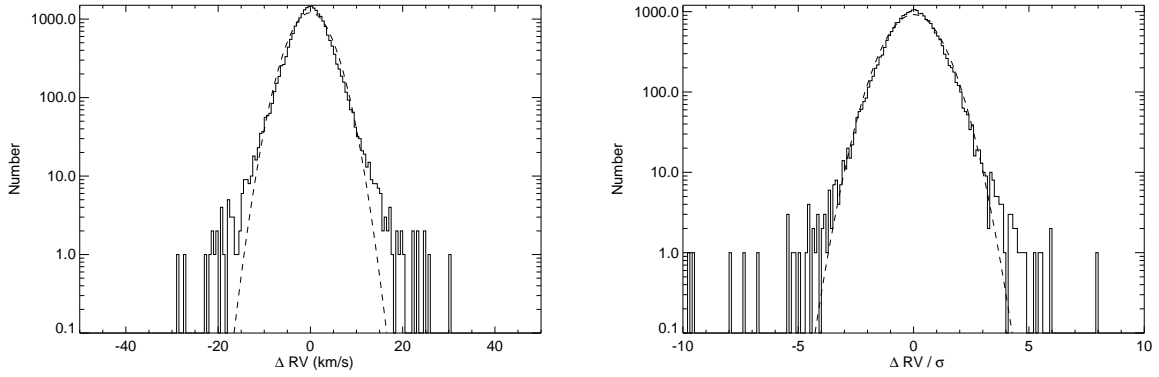


Fig. 3.—: Posterior distributions for a uniform (solid line) and linear (dashed line) distribution of a , respectively.

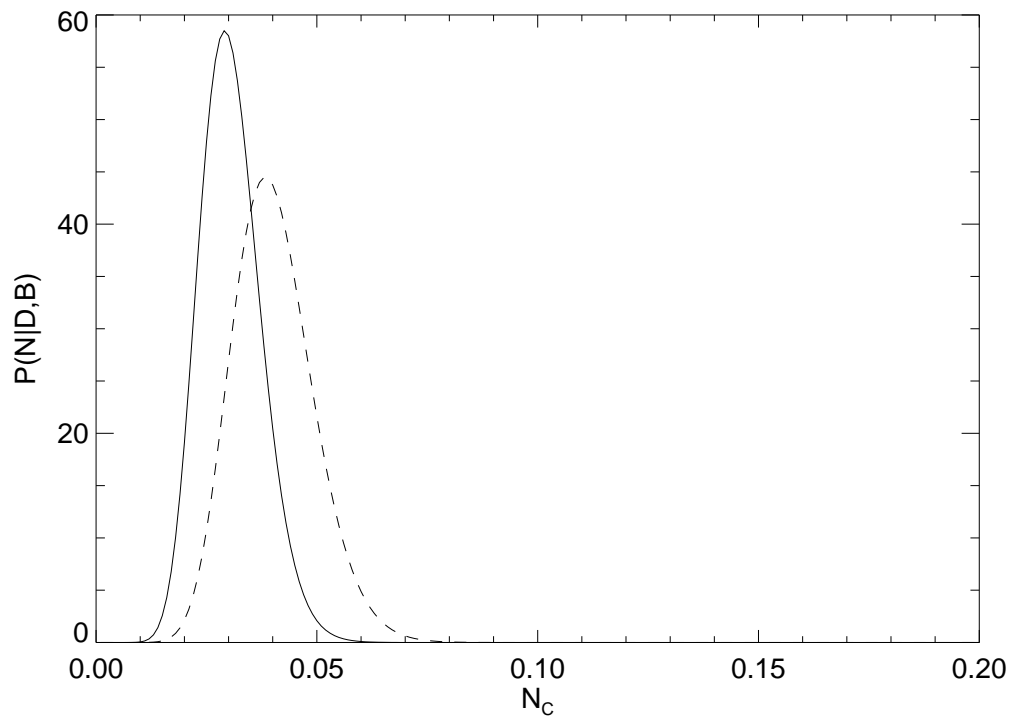


Fig. 4.— Values of the close binary fraction and total binary fraction given in Section 4 and shown in tabular format in Table 4 along with best fit line for each fraction and total binary fraction.

